Received: 31 January 2021 | Revised: 24 May 2021 | Accepted: 29 May 2021

DOI: 10.1002/mrc.5183

SPECIAL ISSUE RESEARCH ARTICLE

WILEY

Solid-state nuclear magnetic resonance of spin-9/2 nuclei ^{115}In and ^{209}Bi in functional inorganic complex oxides

Kent J. Griffith | **Fenghua Ding** | **Steven Flynn**

Department of Chemistry, Northwestern University, Evanston, Illinois, USA

Correspondence
Kent J. Griffith, Department of Chemistry, Northwestern University, 2145 Sheridan Road, Evanston, IL 60208, USA.
Email: kent.griffith@northwestern.edu

Funding information
Basic Energy Sciences

Abstract

Indium and bismuth are technologically important elements, in particular as oxides for optoelectronic applications. ^{115}In and ^{209}Bi are both $I = 9/2$ nuclei with high natural abundances and moderately high frequencies but large nuclear electric quadrupole moments. Leveraging the quadrupolar interaction as a measure of local symmetry and polyhedral distortions for these nuclei could provide powerful insights on a range of applied materials. However, the absence of reported nuclear magnetic resonance (NMR) parameters on these nuclei, particularly in oxides, hinders their use by the broader materials community. In this contribution, solid-state ^{115}In and ^{209}Bi NMR of three recently discovered quaternary bismuth or indium oxides are reported, supported by density functional theory calculations, numerical simulations, diffraction and additional multinuclear (^{27}Al, ^{69,71}Ga, and ^{121}Sb) solid-state NMR measurements. The compounds $LiIn_2SbO_6$, $BiAlTeO_6$, and $BiGaTeO_6$ are measured without special equipment at 9.4 T, demonstrating that wideline techniques such as the QCPMG pulse sequence and frequency-stepped acquisition can enable straightforward extraction of quadrupolar tensor information in $I = 9/2$ ^{115}In and ^{209}Bi even in sites with large quadrupolar coupling constants. Relationships are described between the NMR observables and local site symmetry. These are amongst the first reports of the NMR parameters of ^{115}In, ^{121}Sb, and ^{209}Bi in oxides.

1 | INTRODUCTION

Bismuth- and indium-based complex oxides, that is, oxides containing multiple metal cations, are important functional inorganic materials with a central role in many optoelectronic and energy-related applications. Tin-doped bixbyite indium oxide (In_2O_3) is an n-type transparent conducting oxide[1–3] used in display technology,[4,5] electrochromic smart windows,[6–8] and photovoltaics.[9–11] Complex indium-containing oxides are being developed for the next generation of electronic materials.[12–16] Lithium indium oxides have been studied as prospective solid electrolytes for all-solid-state lithium-ion batteries.[17–19] Substituted versions of fluorite bismuth oxide (δ-Bi_2O_3)[20–23] and Aurivillius-type mixed-metal bismuth oxides[20,24,25] host some of the highest known oxygen-ion conductivities. Bismuthate glasses are nontoxic candidates to replace lead oxide in zero-stress optic materials.[26,27] The stereochemically active lone pair in Bi^{3+} can lead to noncentrosymmetric structures with useful optoelectronic and ferroic properties.[28–32]

Given the range of technological applications and frequently cation-mixed and/or poorly diffracting nature of bismuth and indium oxides, it is desirable to develop alternative metrologies to study their atomic environments. ^{115}In and ^{209}Bi solid-state nuclear magnetic

resonance (NMR) spectroscopy could, in principle, offer additional insights into the local coordination, symmetry, and ionic/polyhedral dynamics. The quadrupolar interaction, specifically, yields information on the spherical (C_Q) and axial (η_Q) symmetry.[33] Both nuclei are spin 9/2 with moderate gyromagnetic ratios ($\gamma_{^{115}In} = 5.8972 \times 10^7$ rad s^{-1} T^{-1}; $\gamma_{^{209}Bi} = 4.3750 \times 10^7$ rad s^{-1} T^{-1}), large nuclear electric quadrupole moments ($Q_{^{115}In} = 77.2(5)$ fm^2; $Q_{^{209}Bi} = -51.6$ (2) fm^2), and high natural abundances (^{115}In = 95.71%; ^{209}Bi = 100%).[34,35] Note that ^{113}In is also spin 9/2 with nearly identical nuclear properties ($\gamma_{^{113}In} = 5.8845 \times 10^7$ rad s^{-1} T^{-1}; $Q_{^{113}In} = 76.1(5)$ fm^2); however, it comprises only 4.29% natural abundance and is thus disfavored. An analogy must be drawn to ^{93}Nb, the only other stable, odd-proton $I = 9/2$ nucleus (*nota bene*, there are several odd-neutron $I = 9/2$ nuclides—^{73}Ge, ^{83}Kr, ^{87}Sr, and ^{179}Hf—but these have substantially lower gyromagnetic ratios). ^{93}Nb has found wider use than its $^{(113)/115}$In and ^{209}Bi counterparts, primarily owing to its smaller nuclear quadrupole moment ($Q_{^{93}Nb} = -32$ (2) fm^2). Combined with its slightly higher frequency ($\gamma_{^{93}Nb} = 6.5674 \times 10^7$ rad s^{-1} T^{-1}) and 100% natural abundance, ^{93}Nb has been used to provide insights on a wide range of materials.[36–41]

Owing to quadrupolar broadening, ^{115}In and ^{209}Bi NMR studies are infrequent. Both nuclei have been studied in a number of halide systems[42–49] and molecular compounds.[48–53] Reports on oxides are exceedingly rare. A pair of very recent reports suggests growing interest in this area.[16,54] Yamada et al. carried out field-swept ^{115}In NMR to determine the quadrupolar coupling parameters of the two indium sites in In_2O_3,[54] complementing the values determined via nuclear quadrupolar resonance (NQR) spectroscopy in the literature[55]; chemical shift information was not determined. Huang et al. employed ^{115}In NMR to study amorphous indium gallium oxide processed with varying polyvinyl alcohol contents. In the latter study, a distinct ^{115}In signal was detected and observed to narrow slightly with polyvinyl alcohol, but no NMR parameters could be extracted.[16] It is clear that there is a need to establish structure–spectral relationships for these important inorganic species, particularly in oxide local environments. The initial focus of this work was to demonstrate the applicability of ^{115}In and ^{209}Bi NMR to oxides, but it is noted that this report is also one of the first to describe ^{121}Sb NMR of an oxide material.[56]

For quadrupolar nuclei, it is generally desired to acquire spectra at the highest available field, B_0, to minimize the breadth of the central-transition static powder lineshape, $\Delta\nu_{CT}$, which is given from second-order perturbation theory as follows:

$$\Delta\nu_{CT} = \left(\frac{3C_Q}{2I(2I-1)}\right)^2 \cdot \left(\frac{\left(\eta_Q^2 + 22\eta_Q + 25\right)(I(I+1) - 3/4)}{144\nu_L}\right), \quad (1)$$

where C_Q is the quadrupolar coupling constant, η_Q is the quadrupolar asymmetry parameter, and ν_L is the Larmor frequency, which is proportional to B_0.[57] Fortunately, in the case of $I = 9/2$ nuclei such as ^{115}In and ^{209}Bi, the central transition linewidths are relatively narrow (for a given C_Q) due to the I-dependence of Equation 1.

The central transition (CT, $m_I = +1/2 \leftrightarrow -1/2$) of a noninteger quadrupolar nucleus is only affected by second-order quadrupolar effects while the eight satellite transitions (STs) in $I = 9/2$ nuclei ($m_I = \pm 1/2 \leftrightarrow \pm 3/2$, $\pm 3/2 \leftrightarrow \pm 5/2$, $\pm 5/2 \leftrightarrow \pm 7/2$, $\pm 7/2 \leftrightarrow \pm 9/2$) are affected by first-, second-, and third-order quadrupolar interactions, contributing to the (ultra-)wide powder patterns expected for full (CT and ST) quadrupolar environments of ^{115}In and ^{209}Bi NMR. While second-order perturbation theory is sufficient for many quadrupolar NMR studies, numerous examples have emerged demonstrating the significance of higher order effects.[58–65] The rule of thumb for the breakdown of second-order perturbation theory and the emergence of third-order effects is when the quadrupolar frequency ν_Q given by the following

$$\nu_Q = \left(\frac{3C_Q}{2I(2I-1)}\right), \quad (2)$$

approaches 10% of the Larmor frequency ν_L.[66] Widdifield et al. showed that even under these conditions, second-order theory would introduce underestimation errors in C_Q and δ_{iso}.[60] For large values of ν_Q, the line between NMR and NQR is blurred.[67,68] The exceptionally large nuclear electric quadrupole moments of ^{113,115}In and ^{209}Bi—the largest of all main group elements—are expected to lead to noticeable third-order effects on the satellite transitions of these nuclei in distorted environments.

In this report, the ^{115}In and ^{209}Bi solid-state NMR spectra and quadrupolar parameters of three recently discovered complex oxides ($LiIn_2SbO_6$, $BiAlTeO_6$, and $BiGaTeO_6$; Figure 1) are examined via (ultra-)wideline NMR, periodic density functional theory (DFT) calculations, and numerical modeling. $LiIn_2SbO_6$ is a rutile-like structure with a channel arrangement that is unique amongst rutile phases (Figure 1a).[19] $BiAlTeO_6$ and $BiGaTeO_6$ are isostructural layered compounds with alternating pure BiO_6 and mixed, ordered MO_6/TeO_6 (M = Al, Ga) (Figure 1b).[31] Collection of the broad

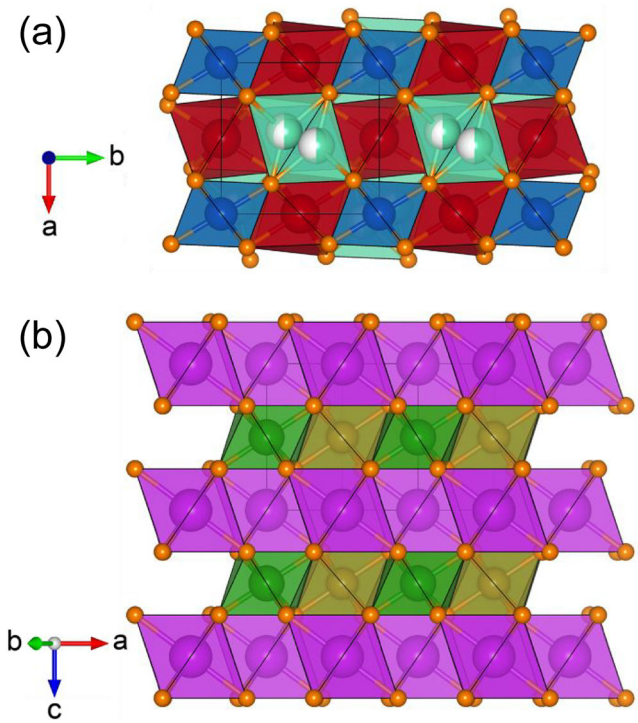

FIGURE 1 Crystal structures of (a) rutile-like $LiIn_2SbO_6$ and (b) layered Bi*M*TeO_6 (*M* = Al, Ga). Li^+ in teal, In^{3+} in red, Sb^{5+} in dark blue, Bi^{3+} in magenta, M^{3+} in green, Te^{6+} in gold, O^{2-} in orange

(>15 MHz) NMR spectra is facilitated by signal enhancement from the quadrupolar Carr–Purcell–Meiboom–Gill (QCPMG) pulse sequence in combination with frequency-stepped acquisition, also known as the variable-offset cumulative spectrum (VOCS)[69] approach. The results are described in the context of the very different local symmetry and coordination environments of indium and bismuth in these examples. A new synthetic route is developed to prepare a bulk sample of crystalline $BiAlTeO_6$ suitable for NMR. Chemical shift and quadrupolar parameters of ^{27}Al, ^{71}Ga, and ^{121}Sb NMR are also investigated and correlated to the local geometry of these cations.

2 | EXPERIMENTAL

2.1 | Synthesis

$LiIn_2SbO_6$, $BiAlTeO_6$, and $BiGaTeO_6$ were synthesized from high-temperature solid-state or flux methods.[19,31] Li_2CO_3 (Aldrich, 99.999%), Na_2CO_3 (Aldrich, 99.0%), In_2O_3 (Alfa Aesar, 99.994%), Sb_2O_3 (Aldrich, 99%), Bi_2O_3 (Aldrich, 99.9%), Al_2O_3 (Aldrich, 99.9%), Ga_2O_3 (Aldrich, 99.9%), and TeO_2 (Aldrich, 99.9%) precursors were used as received. $H_2TeO_4{\cdot}2H_2O$ (Aldrich, 99.6%) was converted to amorphous TeO_3 through a preheating step at 673 K for 12 h in air. The reagents were ground together in an agate mortar and pestle until homogenous. $LiIn_2SbO_6$ was prepared by annealing the stoichiometric pelletized reactants in a Pt crucible in air at 1173 K for 8 h followed by 1473 K for 20 h with an intermediate regrinding. Attempts to prepare single-phase $BiAlTeO_6$ via solid-state reaction with stoichiometric quantities of Al_2O_3, Bi_2O_3, and TeO_3 (or TeO_2) were unsuccessful, as reported.[31] Thus, a Na_2CO_3–TeO_2 flux method demonstrated to produce single crystals[31] of $BiAlTeO_6$ was modified to prepare a larger quantity for this work. A mixture 1:4:1 mole ratio of Na_2CO_3:TeO_2:Bi_2O_3 was placed in an alumina crucible, which provided the source of Al for $BiTeAlO_6$. The crucible was heated to 973 K, held for 5 h as a melt, cooled to 673 K at a rate of 0.1 K min^{-1}, and then quenched to room temperature on the bench. $BiGaTeO_6$ was prepared by heating a pellet of Bi_2O_3, Ga_2O_3, and TeO_3 in a Pt crucible in air for a total of 40 h at 973 K with intermediate regrindings.

2.2 | Diffraction

Powder X-ray diffraction (XRD) patterns were recorded in transmission mode with a STOE Stadi P diffractometer and Cu Kα radiation. Finely ground sample powders were loaded between two sheets of Kapton tape. Diffraction patterns were recorded from 5 to 80° 2θ while the sample rotated to improve powder averaging (*nota bene*, data are displayed from 15° to 75° 2θ to more clearly show the observed reflections). Calculated patterns correspond to entries in the Inorganic Crystal Structure Database (ICSD): $LiIn_2SbO_6$ (collection code 1976010), $BiAlTeO_6$ (collection code 21784), and $BiGaTeO_6$ (collection code 21785).

2.3 | Solid-state NMR

NMR spectra were recorded in a 9.4-T static magnetic field with a Bruker Avance III spectrometer and a 4.0-mm Bruker HX probe with the exception of ^{23}Na and fast magic-angle spinning (MAS) ^{69,71}Ga measured with a 1.6-mm Phoenix HFX probe. MAS and static ^{27}Al spectra were acquired with a Bloch decay ($\pi/2$–acq.) pulse sequence and a 1.3-μs excitation pulse corresponding to the π/2 pulse optimized on α-Al_2O_3. For ^{27}Al, a recycle delay of 6.25 s was used, corresponding to $5T_1$, and 192 scans were summed. ^{69}Ga MAS and static NMR spectra were recorded with a Hahn-echo ($\pi/2$–τ_1–π–τ_2–acq.) pulse sequence with a rotor-synchronized (MAS) or 10-μs (static) interpulse delay. ^{69,71}Ga spectra were collected

with either a Bloch decay pulse sequence or a Hahn-echo pulse sequence with rotor synchronization or, for static Hahn-echo spectra, a 10-μs interpulse delay. For static and 10–15 kHz MAS ^{69}Ga and ^{71}Ga recorded on the 4.0 mm probe, a $\frac{\pi/2}{(I+\frac{1}{2})} = (\pi/4)_{\text{liquid}}$ excitation pulse of 2.2 μs was applied, the recycle delays were 2 s ($\sim 2\,T_1$), and 3072–12,288 scans (^{69}Ga) or 256–560 scans (^{71}Ga) were summed. For ^{69}Ga and ^{71}Ga spectra collected at 35 kHz MAS with the 1.6-mm probe, an excitation pulse of 1.0 μs was applied; 56,480 scans with a recycle delay of 1 s were summed for ^{69}Ga, and 17,800 scans with a recycle delay of 3 s were summed for ^{71}Ga. ^{23}Na MAS NMR was recorded with a rotor-synchronized Hahn-echo, a 1.1 μs π/2 pulse, a 10-s recycle delay, and by summing 128 scans. Static ^{115}In, ^{121}Sb, and ^{209}Bi spectra were recorded with a frequency-stepped quadrupolar QCPMG approach with excitation and refocusing pulses of 1.0- and 2.0-μs, respectively, and a spikelet spacing of 5 kHz. The excitation and refocusing pulse lengths were determined by maximizing the ^{209}Bi central transition signal in $BiGaTeO_6$. For ^{115}In QCPMG, 21 echoes were captured in each free induction decay, 186 spectra were collected with transmitter offset steps of 100 kHz, the recycle delay was 0.1 s, and 256 scans were summed at each offset frequency. For ^{209}Bi QCPMG in $BiAlTeO_6$, 21 echoes were captured in each free induction decay, 145 spectra were collected with transmitter offset steps of 125 kHz, the recycle delay was 0.05 s, and 16,384 scans were summed at each offset frequency. For ^{209}Bi QCPMG in $BiGaTeO_6$, 11 echoes were captured in each free induction decay, 133 spectra were collected with transmitter offset steps of 125 kHz, the recycle delay was 0.05 s, and 8192 scans were summed at each offset frequency. Solid NaCl at 7.2 ppm,[70] α-Al_2O_3 (corundum) at 16.0 ppm ($C_Q = 2.38$ MHz),[57,71] 1.0-M Ga $(NO_3)_{3(aq.)}$ at 0.0 ppm,[72] 0.1-M In $(NO_3)_3$ in 0.5-M HNO_3 at 0.0 ppm,[51,72], and saturated Bi $(NO_3)_3$ in concentrated HNO_3 at 0.0 ppm[72] were used as NMR shift references.

2.4 | Spectral simulations

^{27}Al, ^{69}Ga, and ^{71}Ga MAS and static solid-state NMR spectra were simulated with second-order perturbation theory in the solid lineshape analysis (SOLA) program within TopSpin 3.6.1. Static ^{113}In, ^{115}In, ^{121}Sb, and ^{209}Bi spectra were modeled with the "Quadrupolar Exact Software" (QUEST) numerical simulation program, which treats the combined Zeeman–quadrupole Hamiltonian exactly.[63] MagresView (v1.6.2) was used to visualize tensor orientations and calculate Euler angles.[73]

2.5 | NMR conventions

In this study, the Haeberlen convention is used to describe the chemical shift tensor with the isotropic shift $\delta_{iso} = \frac{\delta_{XX}+\delta_{YY}+\delta_{ZZ}}{3}$; chemical shift anisotropy $\delta_{CSA} = \delta_{ZZ} - \delta_{iso}$; and the shift asymmetry $\eta_{CSA} = \frac{\delta_{YY}-\delta_{XX}}{\delta_{ZZ}-\delta_{iso}}$. In this definition, the principal components of the shift tensor are ordered such that $|\delta_{ZZ} - \delta_{iso}| \geq |\delta_{XX} - \delta_{iso}| \geq |\delta_{YY} - \delta_{iso}|$. The above definition of δ_{CSA} is sometimes referred to as the reduced anisotropy, which is equal to 2/3 of the "full" anisotropy $\Delta\delta = \delta_{ZZ} - \frac{\delta_{XX}+\delta_{YY}}{2}$ used by some authors and programs. The quadrupolar coupling constant C_Q is defined by the nuclear quadrupole moment Q and the largest principal component V_{ZZ} of the electric field gradient (EFG) at the nucleus according to $C_Q = \frac{eQV_{ZZ}}{h}$, where e is the electric charge and h is Planck's constant. The quadrupolar asymmetry parameter η_Q is defined by the EFG tensor components as $\eta_Q = \frac{V_{XX}-V_{YY}}{V_{ZZ}}$, with components ordered such that $|V_{ZZ}| \geq |V_{YY}| \geq |V_{XX}|$. The relative orientations of the chemical shift and quadrupolar tensors are defined by a set of Euler angles α, β, and γ defined here in the (ZYZ) Rose convention.

2.6 | Ab initio calculations

Chemical shielding and EFG calculations were performed with the gauge-including projector augmented-wave (GIPAW) approach in the planewave pseudopotential code CASTEP.[74–77] The calculations used the Perdew–Burke–Ernzerhof (PBE) exchange–correlation functional[78] and Vanderbilt ultrasoft pseudopotentials[79] with the default Koelling–Harmon scalar relativistic treatment.[80] $LiIn_2SbO_6$, $BiAlTeO_6$, and $BiGaTeO_6$ crystal structures were used as starting models.[19,31] Prior to the NMR calculations, atomic positions and lattice parameters were optimized until the force on any atom was smaller than 1 meV Å^{-1}. All calculations used a planewave energy cutoff energy of 700 eV and a Monkhorst–Pack[81] grid with a spacing finer than $2\pi \times 0.03$ Å^{-1} to sample the Brillouin zone. Anisotropic NMR parameters were used as the starting point to fit the experimental spectra.

3 | RESULTS AND DISCUSSION

3.1 | Synthesis and diffraction

Crystalline samples of $LiIn_2SbO_6$ and $BiGaTeO_6$ were synthesized by high-temperature solid-state methods while $BiAlTeO_6$ was synthesized from a flux to overcome

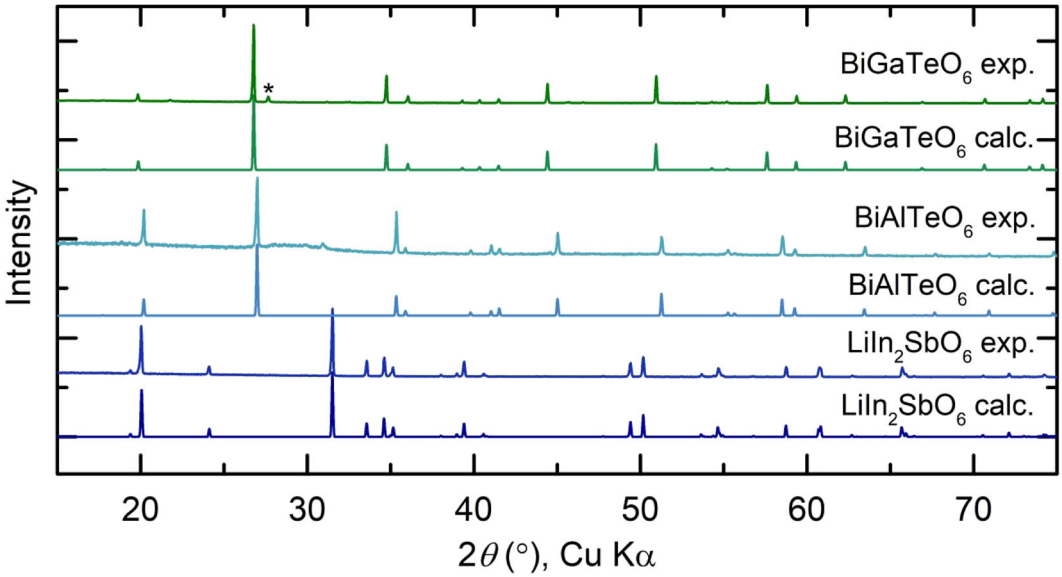

FIGURE 2 Experimental and calculated X-ray diffraction patterns of $LiIn_2SbO_6$, $BiAlTeO_6$, and $BiGaTeO_6$. The asterisk in the pattern of the $BiGaTeO_6$ sample denotes an impurity peak assigned to $Bi_2Te_2O_7$

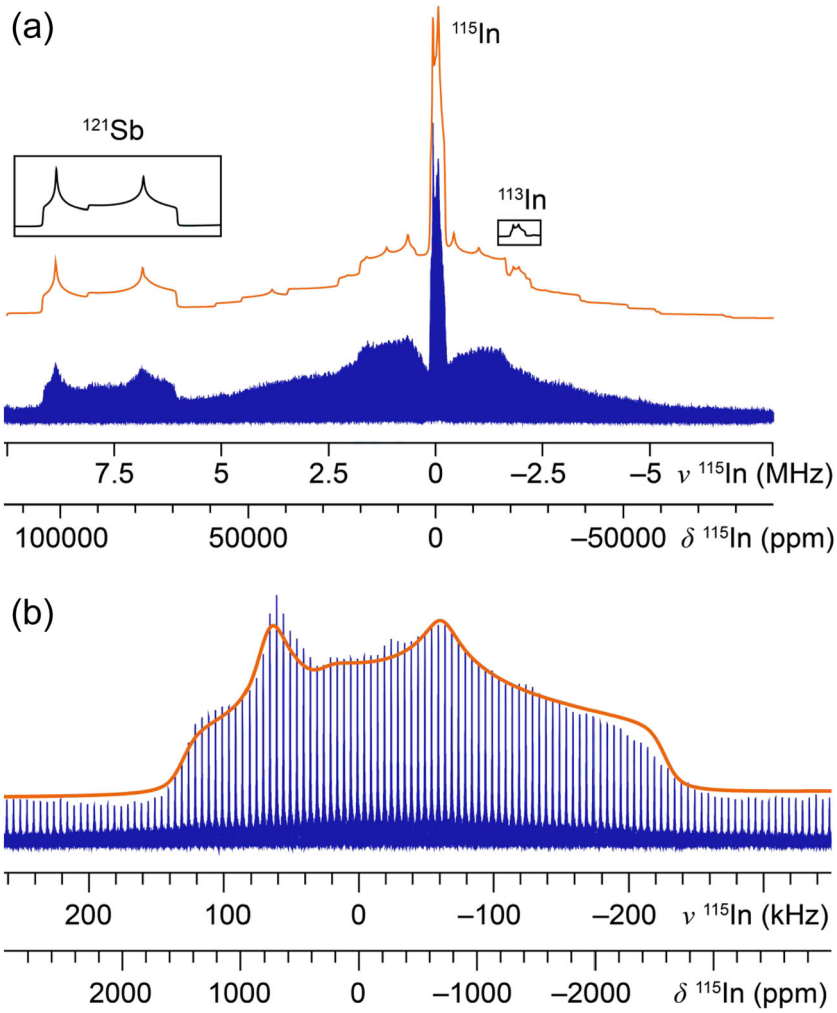

FIGURE 3 ^{115}In nuclear magnetic resonance (NMR) of $LiIn_2SbO_6$. (a) Full spectral width including the ^{115}In central and satellite transitions, ^{121}Sb central transition at high frequency, and the ^{113}In central transition at low frequency (not experimentally resolved). (b) ^{115}In central transition region only. Experimental data in blue, full simulations in orange, ^{121}Sb and ^{113}In contributions to the overall lineshape inset in black. The ppm scale is relative to the ^{115}In reference compound

substantial impurities observed from the previously described method.[31] Laboratory powder XRD confirmed the crystal structure and crystalline purity of each sample (Figure 2). A broad background component is visible in the diffraction pattern of the $BiAlTeO_6$ sample. Based on the flux composition, this scattering contribution is attributed to amorphous sodium tellurates.

3.2 | Solid-state NMR of $LiIn_2SbO_6$

A wideline solid-state ^{115}In NMR spectrum of $LiIn_2SbO_6$ was recorded by collecting frequency-stepped subspectra covering an excitation range of more than 18 MHz (Figures 3 and S1–S3). In addition to signals from ^{115}In, the broadband spectrum also overlaps the ^{121}Sb and ^{113}In Larmor frequencies. While the ST intensity was visible for >15 MHz (Figure 3a), the ^{115}In CT linewidth was only ca. 400 kHz (Figures 3b and S1). At high frequencies, a quadrupolar CT lineshape from the ^{121}Sb site was clearly distinguished (Figures 3a, 4, and S2). The CT pattern of ^{121}Sb is an order-of-magnitude broader than the CT of ^{115}In due not only to the higher C_Q of the former in this sample but also the lower spin quantum number of ^{121}Sb ($I = 5/2$, see Equation 1). The minor signal expected from ^{113}In at low frequency was not readily observed (Figures 3a and S3).

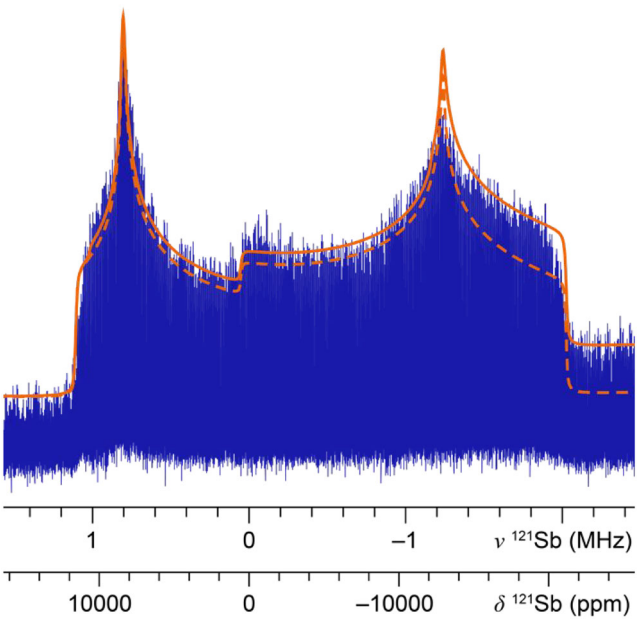

FIGURE 4 ^{121}Sb nuclear magnetic resonance (NMR) of $LiIn_2SbO_6$. Experimental data in blue, spectral simulations in orange. The dashed orange trace is the pure ^{121}Sb contribution while the solid orange trace is from the full simulation (see Figure 3) including ^{115}In satellite transition intensity, which contributes to the lineshape on the low-frequency side

Planewave DFT calculations of the shielding and quadrupolar tensors provided a helpful starting point for spectral fitting. Full (CT and ST) simulations of the experimental lineshape yielded a ^{115}In quadrupolar coupling constant of 54.5(10) MHz with an asymmetry of 0.53(2) (Table 1). Few ^{115}In satellite transition discontinuities were visible, but the simulation and experiment are in reasonable agreement for the central transition features and for the overall satellite lineshape. A ^{115}In isotropic shift of 130(20) ppm was determined, but the large quadrupolar interaction precluded the extraction of anisotropic chemical shift parameters at this moderate B_0 field (9.4 T). The calculated chemical shift anisotropy (Table 1) had no effect on the lineshape. The ^{121}Sb signal was simulated with a C_Q of 89(1) MHz and an η_Q of 0.238 (5). Additional details concerning the ^{115}In and ^{121}Sb variable-offset QCPMG spectral representations are given in Figures S1 and S2, respectively.

3.3 | Structure–spectral relationships in $LiIn_2SbO_6$

The single crystallographically unique indium site in $LiIn_2SbO_6$ is a distorted InO_6 octahedron with room-temperature bond-lengths varying from 2.10 to 2.26 Å and severely distorted bond angles.[19] Despite these first-shell distortions, the magnitude of C_Q in $LiIn_2SbO_6$ (54.5 (10) MHz) is substantially smaller than either indium site in bixbyite In_2O_3 (In(1) = 183(2) MHz; In(2) = 126 (2) MHz).[54,55] Nevertheless, the experimental ^{115}In C_Q in the quaternary oxide is substantially larger than the DFT-predicted value. A similar phenomenon was observed for ^{121}Sb. The intermediate ^{115}In and ^{121}Sb asymmetry parameters are consistent with the lack of axial symmetry at the indium or antimony site.

One possible explanation for the deviation between the calculated and experimental results relates to disorder on the lithium site. Lithium coordination in $LiIn_2SbO_6$ was previously probed by ^{6}Li and ^{7}Li NMR where it was determined that the unique tunnel pattern of this rutile-like structure hosts lithium ions in (split) tetrahedral sites.[19] This finding ran counter to a previous proposal that $LiIn_2SbO_6$ is simply a cation-ordered variant of $LiSbO_3$ with octahedral LiO_6 sites. The ^{6,7}Li NMR, however, is unable to resolve the question of whether it is disordered (statically or dynamically) in the split tetrahedral site, which may affect the indium and antimony via next-nearest-neighbor (NNN) interactions. It is also possible that the computed C_Q parameters for ^{115}In and ^{121}Sb in $LiIn_2SbO_6$ are underestimated, which is a known issue in a variety of systems and with different quadrupolar nuclei.[38,82,83]

TABLE 1 Experimental and calculated ^{115}In and ^{121}Sb nuclear magnetic resonance (NMR) parameters of $LiIn_2SbO_6$

Nucleus	Source	σ_{iso} or δ_{iso} (ppm)[a]	δ_{CSA} (ppm)	η_{CSA}	C_Q (MHz)	η_Q	α,β,γ (°)
^{115}In $LiIn_2SbO_6$	Calculated	$\sigma_{iso} = 3331$	−50.4	0.89	39.3	0.46	26,90,3
	Experimental[b]	$\delta_{iso} = 130(20)$	n/d	n/d	54.5(10)	0.53(2)	n/d
^{121}Sb $LiIn_2SbO_6$	Calculated	$\sigma_{iso} = 2388$	−96.6	0.03	58.4	0.43	0,1,0
	Experimental[b]	$\delta_{iso} = 350(20)$	n/d	n/d	89(1)	0.238(5)	n/d

[a]In the absence of additional ^{115}In or ^{121}Sb shift measurements, it is not yet possible to reliably convert the calculated shieldings to the experimentally observed isotropic shifts. However, the values here may prove useful in deriving future relationships.
[b]Estimated uncertainty in the fit given in parentheses.

3.4 | Solid-state NMR of Bi*M*TeO$_6$ (*M* = Al, Ga)

The frequency-stepped VOCS method with QCPMG pulses was also used to record (ultra-)wideline CT and partial ST spectra of $BiAlTeO_6$ and $BiGaTeO_6$ covering more than 16 MHz (Figures 5 and S4). Both samples exhibit ^{209}Bi CT that are greater than 1 MHz in breadth (Figure S5). Numerous distinct satellite transition features were clearly resolved in the ultra-wideline spectra across the entire measured frequency range.

Once again, DFT calculations provided a valuable basis for approaching the spectral fitting. As in the case of the ^{115}In spectrum, the calculated shift anisotropy suggested that it would have no impact on the simulated ^{209}Bi linewidth at 9.4 T, and so the number of variable fitting parameters could be reduced. Note that a previous study of bismuth compounds (oxyhalides, nitrate pentahydrate, triflate, and acetate) observed chemical shift anisotropy values that were typically an order-of-magnitude larger than the calculated values for the bismuth oxides here.[48] The quadrupolar tensor parameters were adjusted to match the discontinuities in the powder lineshape, and the quadrupolar coupling values from DFT were found to be within 5% of those determined experimentally (Table 2).

NMR spectra of the quadrupolar *M*-site cations in Bi*M*TeO$_6$ were measured as further probes of the atomic structure models. ^{27}Al MAS NMR of $BiAlTeO_6$ revealed a single pseudo-Voigt lineshape with a center of gravity at 18.5 ppm (Figure 6). The calculated C_Q of 2.0 MHz yields a narrower line (by about a factor of two) than the one observed; however, the calculated C_Q is consistent with the breadth of the spinning sideband manifold (~670 kHz). Assuming this C_Q magnitude, which equates to a quadrupolar shift of ca. 2.2 ppm, the isotropic shift is 20.7 ppm, but the estimated error in the shift is given at 3 ppm to account for uncertainty in the relatively featureless CT lineshape (Table 3). A static ^{27}Al NMR spectrum gave a featureless resonance with a full-width at half-maximum of about 150 ppm, which did not add any

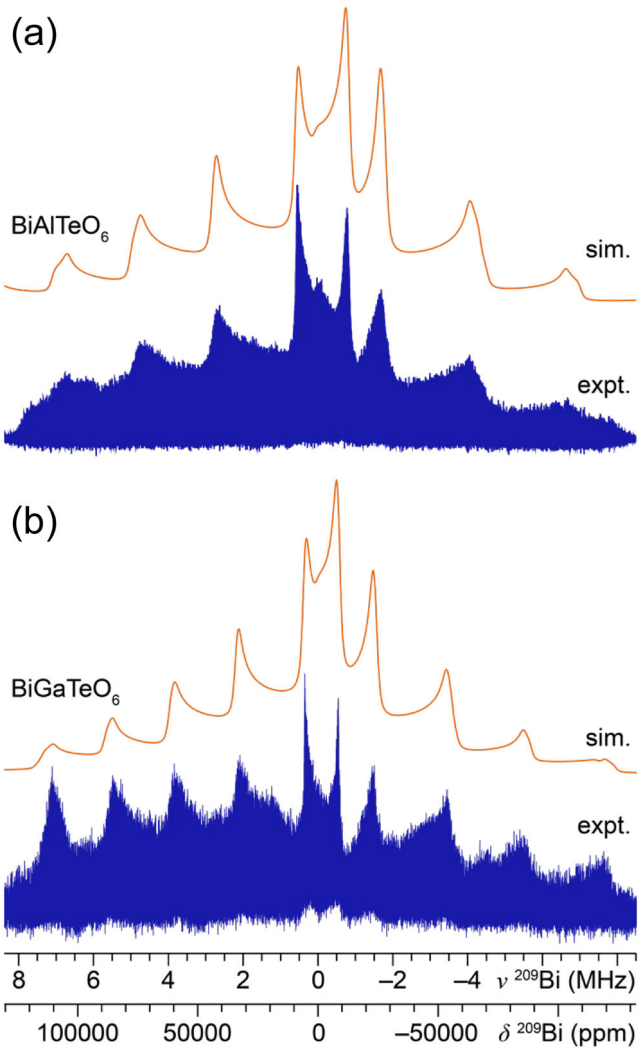

FIGURE 5 ^{209}Bi nuclear magnetic resonance (NMR) of (a) $BiAlTeO_6$ and (b) $BiGaTeO_6$. Experimental data in blue, spectral simulations in orange

information (not shown). ^{69}Ga and ^{71}Ga static spectra of $BiGaTeO_6$ showed powder lineshapes characteristic of second-order quadrupolar broadening with near axial symmetry (Figure 7). The gallium spectra contain a number of overlapping sidebands at moderate MAS rates

TABLE 2 Experimental and calculated ^{209}Bi nuclear magnetic resonance (NMR) parameters of $BiAlTeO_6$ and $BiGaTeO_6$

Nucleus	Source	σ_{iso} or δ_{iso} (ppm)[a]	δ_{CSA} (ppm)	η_{CSA}	C_Q (MHz)	η_Q	α,β,γ (°)
^{209}Bi $BiAlTeO_6$	Calculated	$\sigma_{iso} = 6192$	−137	0.00	106.5	0.00	1,0,116
	Experimental[b]	$\delta_{iso} = 1300(500)$	n/d	n/d	110(2)	0.03(3)	n/d
^{209}Bi $BiGaTeO_6$	Calculated	$\sigma_{iso} = 6091$	−120	0.00	93.9	0.00	19,0,142
	Experimental[b]	$\delta_{iso} = 1500(500)$	n/d	n/d	90(2)	0.02(2)	n/d

[a]In the absence of additional ^{209}Bi shift measurements, it is not yet possible to reliably convert the calculated shieldings to the experimentally observed isotropic shifts. However, the values here may prove useful in deriving future relationships.
[b]Estimated uncertainty in the fit given in parentheses.

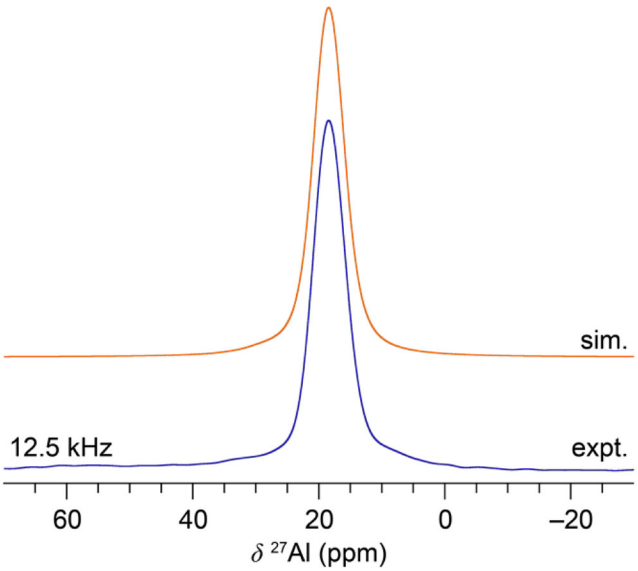

FIGURE 6 ^{27}Al MAS nuclear magnetic resonance (NMR) spectrum of $BiAlTeO_6$. Experimental data in blue, spectral simulation in orange

(10–15 kHz) that are much smaller than the CT linewidths; this problem is alleviated for ^{71}Ga but not entirely for ^{69}Ga at 35 kHz MAS (Figure 7). In each case, the features under static and variable MAS rates could be readily simulated with second-order perturbation theory (Table 3). The two gallium nuclei have a relative nuclear quadrupole moment ratio of $^{69}Ga/^{71}Ga = 1.60$, so collection of both datasets provides additional constraints for the simulations.[35] The complementary datasets also enabled the estimation of the chemical shift anisotropy, albeit data from a higher B_0 field would improve the precision.

Based on the synthesis conditions and the broad feature in the XRD of $BiAlTeO_6$, it was hypothesized that the sample contains amorphous sodium tellurate(s). ^{23}Na MAS NMR supports this hypothesis, showing a broad asymmetric resonance centered around −35 ppm (Figure S6), which is similar to the reported ^{23}Na NMR of $(Na_2O)_x(TeO_2)_{1-x}$ glasses.[86]

3.5 | Structure–spectral relationships in Bi*M*TeO$_6$ (*M* = Al, Ga)

$BiAlTeO_6$ and $BiGaTeO_6$ are isostructural layered compounds with a single crystallographically distinct position for each of the cations. Unlike In^{3+} in $LiIn_2SbO_6$, the Bi^{3+} cations in Bi*M*TeO$_6$ sit in nearly perfect octahedral symmetry with respect to the nearest-neighbor oxygen coordination. All Bi–O distances are identical, and the O–Bi–O bond angles only vary from 87.9° to 92.9°. Thus, considering only the first-shell interactions, bismuth has nearly spherical site symmetry and a small ^{209}Bi C_Q would be expected. Owing to the layered nature and chiral structure of Bi*M*TeO$_6$, the NNN (Figure 8) coordination of bismuth (i.e., $BiAl_6Te_6$ or $BiGa_6Te_6$) should be considered for the origin of the observed (ultra-)wideline CT (Figures 5 and S5). The NNN distances are in a narrow range from 3.844 to 3.846 Å, but the geometry is that of a hexagonal prism. Thus, the $BiAl_6Te_6$ or $BiGa_6Te_6$ units deviate strongly from spherical symmetry; however, there is D_{3h} symmetry with the three-fold axis along the *c* direction (Figure 8). Accordingly, the largest component of the electric field tensor (V_{33}) at the bismuth nucleus is oriented along *c*. The same symmetry properties and V_{33} orientation are true for gallium and, in principle, aluminum. The dominant role of NNN effects in Bi*M*TeO$_6$ are proposed as the explanation for the relatively small ^{209}Bi C_Qs [$BiAlTeO_6$ = 110(2) MHz; $BiGaTeO_6$ = 90(2) MHz] as compared to α-Bi_2O_3 [Bi(1) = 556.7 MHz; Bi(2) = 482.6 MHz][87] with strongly distorted BiO_6 octahedra. Excellent agreement between the calculated and experimentally observed quadrupolar parameters for the bismuth site in Bi*M*TeO$_6$ strengthen the structural model and suggest the absence of significant aperiodic phenomena such as cation disorder. The calculated gallium quadrupolar parameters are underestimated, but this was systematically observed by Middlemiss et al. for a large number of gallates, suggesting an underlying problem that is not unique to $BiGaTeO_6$.[85]

TABLE 3 Experimental and calculated ^{27}Al and ^{69,71}Ga nuclear magnetic resonance (NMR) parameters of $BiAlTeO_6$ and $BiGaTeO_6$

Nucleus	Source	δ_{iso} (ppm)	δ_{CSA} (ppm)	η_{CSA}	C_Q (MHz)	η_Q	α,β,γ (°)
^{27}Al $BiAlTeO_6$	Calculated	29[a]	10.0	0.00	2.02	0.00	78,9,35
	Experimental[b]	21(3)	n/d	n/d	≤2.0	n/d	n/d
^{69,71}Ga $BiGaTeO_6$	Calculated	85[c]	20.3	0.00	^{69}Ga = 8.14;[d] ^{71}Ga = 5.09	0.00	−71,0,147
	Experimental[b]	45(3)	40(20)	n/d	^{69}Ga = 10.7(1);[d] ^{71}Ga = 6.68(6)	0.00(3)	n/d

[a]Calculated ^{27}Al shielding converted to shift according to the expression $\delta_{iso} = m\sigma_{iso} + \sigma_{ref.}$ where $m = -1.027$ and $\sigma_{ref.} = 572.35$ ppm from Seymour et al.[84]
[b]Estimated uncertainty in the fit given in parentheses.
[c]Calculated ^{69,71}Ga shielding converted to shift according to the previous expression where $m = -0.867$ and $\sigma_{ref.} = 1502.63$ ppm from Middlemiss et al.[85]
[d]The ^{69}Ga quadrupolar coupling constant is fixed relative to the ^{71}Ga C_Q according to the ratio of the ^{69}Ga/^{71}Ga nuclear electric quadrupole moments, which is 17.1/10.7 = 1.60.[35]

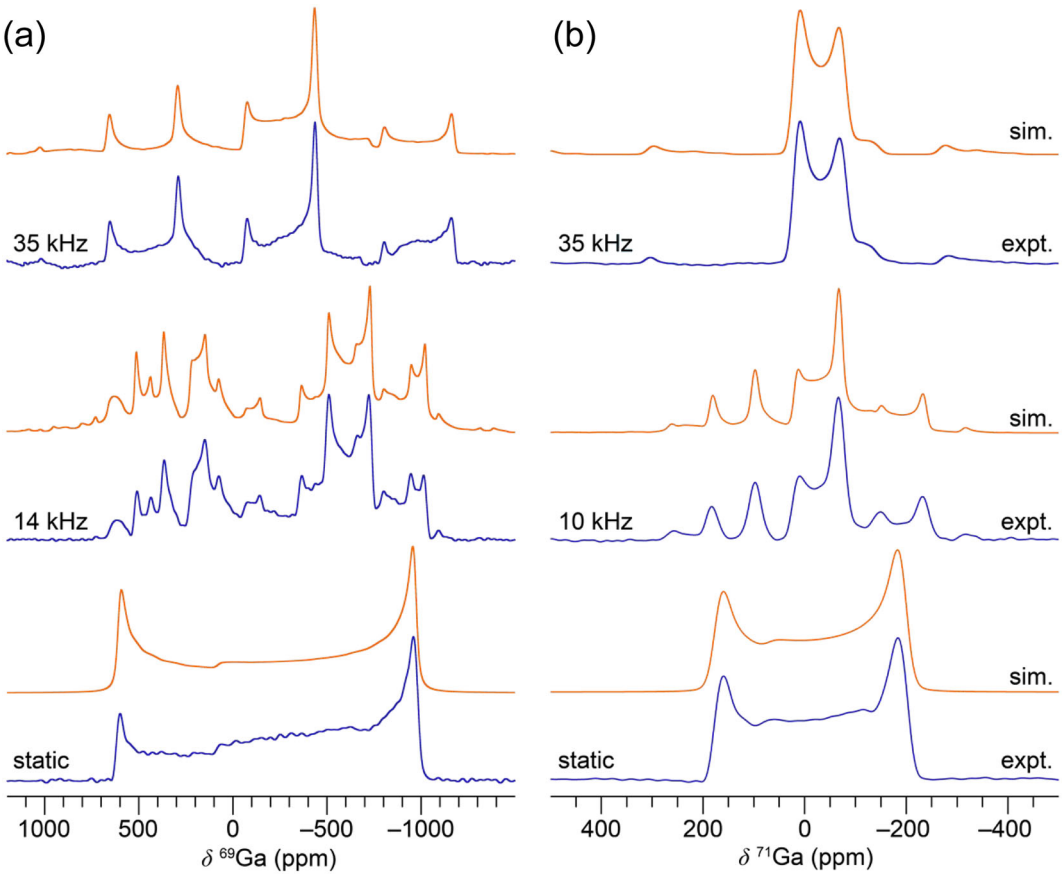

FIGURE 7 (a) ^{69}Ga and (b) ^{71}Ga nuclear magnetic resonance (NMR) of $BiGaTeO_6$. Experimental data in blue, spectral simulations in orange

3.6 | Higher order quadrupolar effects

Third-order quadrupolar interactions are known to affect satellite transition frequencies in strongly quadrupolar systems. Despite ^{115}In having the largest nuclear electric quadrupole moment of the nuclei studied in this work and ^{209}Bi sites possessing the largest C_Qs, it was ^{121}Sb that deviated the most from the high-field approximation. Owing to the relatively small spin quantum number, the ^{121}Sb ($I = 5/2$) nucleus in $LiIn_2SbO_6$ has a ν_Q/ν_L ratio of 0.14. QUEST software was used to simulate all these static spectra with an exact treatment of the Zeeman–quadrupole interaction,[63] but the results suggest that the effects would have been negligible in the spin-9/2 spectra.

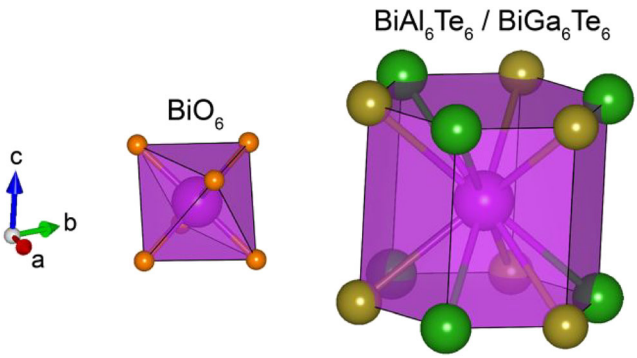

FIGURE 8 First-shell coordination (BiO_6) and second-shell coordination (BiM_6Te_6, M = Al, Ga) in $BiMTeO_6$. A three-fold rotation axis runs parallel to c. Bi^{3+} in magenta, M^{3+} in green, Te^{6+} in gold, O^{2-} in orange

4 | CONCLUSIONS

^{115}In and ^{209}Bi solid-state NMR spectra and quadrupolar tensor quantities were reported for a series of quaternary oxides. These rarely studied $I = 9/2$ nuclei are common in a wide range of technologically important oxide materials, and this work demonstrates that quantitative information regarding first- and second-shell coordination environments can be obtained with standard solid-state NMR tools and approaches. The central transition ^{115}In spectrum of the distorted In^{3+} site in $LiIn_2SbO_6$ was collected in less than 5 min and the ultra-wideline central transition of ^{209}Bi in BiMTeO$_6$ (M = Al, Ga) required only 2–3 h, all at a modest B_0 field of 9.4 T. Satellite transition intensity was measured out to 15–20 MHz with QCPMG for signal enhancement and the VOCS method to overcome excitation bandwidth limitations. Collecting satellite transition data is not routinely necessary but provides more precise quadrupolar coupling parameters and can reveal interesting third-order quadrupolar interaction effects in strongly coupled systems. Though not required, as demonstrated here, automated tuning software/hardware can facilitate the collection of ultra-wideline spectra. Application of adiabatic, wideline, uniform-rate, smooth-truncation (WURST) pulses could further decrease the instrument time in future studies.[88–90] Finally, DFT calculations are particularly powerful as a predictive tool when studying systems with large quadrupolar coupling interactions. Simulations of the expected lineshapes facilitate the design of suitable experiments, for example, echo versus QCPMG, QCPMG spikelet spacing, VOCS spacing, spectrometer time required, and the consequences of different field strengths.

ACKNOWLEDGEMENTS

This work was supported as part of the Joint Center for Energy Storage Research, an Energy Innovation Hub funded by the US Department of Energy, Office of Science, Basic Energy Sciences. This work made use of the IMSERC X-ray and NMR facilities at Northwestern University, which have received support from the Soft and Hybrid Nanotechnology Experimental (SHyNE) Resource (NSF ECCS-2025633), International Institute of Nanotechnology, and Northwestern University. The authors thank Professor Kenneth R. Poeppelmeier, Northwestern University for comments on the manuscript and Can P. Koçer, University of Cambridge for assistance with the DFT calculations.

CONFICT OF INTEREST

The authors declare no competing financial interest.

PEER REVIEW

The peer review history for this article is available at https://publons.com/publon/10.1002/mrc.5183.

DATA AVAILABILITY STATEMENT

Data underlying this manuscript are available for download online (https://doi.org/10.6084/m9.figshare.14478168).

ORCID

Kent J. Griffith https://orcid.org/0000-0002-8096-906X

REFERENCES

[1] R. Bel Hadj Tahar, T. Ban, Y. Ohya, Y. Takahashi, *J. Appl. Phys.* **1998**, *83*, 2631. https://doi.org/10.1063/1.367025

[2] L. Bizo, J. Choisnet, R. Retoux, B. Raveau, *Solid State Commun.* **2005**, *136*, 163. https://doi.org/10.1016/j.ssc.2005.07.009

[3] C. A. Hoel, T. O. Mason, J.-F. Gaillard, K. R. Poeppelmeier, *Chem. Mater.* **2010**, *22*, 3569. https://doi.org/10.1021/cm1004592

[4] C. G. Granqvist, A. Hultåker, *Thin Solid Films* **2002**, *411*, 1. https://doi.org/10.1016/S0040-6090(02)00163-3

[5] U. Betz, M. K. Olsson, J. Marthy, M. F. Escolá, F. Atamny, *Surf. Coat. Technol.* **2006**, *200*, 5751. https://doi.org/10.1016/j.surfcoat.2005.08.144

[6] G. Garcia, R. Buonsanti, A. Llordes, E. L. Runnerstrom, A. Bergerud, D. J. Milliron, *Adv. Opt. Mater.* **2013**, *1*, 215. https://doi.org/10.1002/adom.201200051

[7] C. G. Granqvist, *Thin Solid Films* **2014**, *564*, 1. https://doi.org/10.1016/j.tsf.2014.02.002

[8] A. Maho, C. A. S. Cabezas, K. A. Meyertons, L. C. Reimnitz, S. Sahu, B. A. Helms, D. J. Milliron, A. Maho, C. A. Saez Cabezas, K. A. Meyertons, L. C. Reimnitz, S. Sahu, B. A. Helms, D. J. Milliron, *Chem. Mater.* **2020**, *32*, 8401. https://doi.org/10.1021/acs.chemmater.0c02399

[9] P. Cheng, X. Zhan, *Chem. Soc. Rev.* **2016**, *45*, 2544. https://doi.org/10.1039/C5CS00593K

[10] S. Chen, Y. Wang, L. Zhang, J. Zhao, Y. Chen, D. Zhu, H. Yao, G. Zhang, W. Ma, R. H. Friend, P. C. Y. Chow, F. Gao, H. Yan, *Adv. Mater.* **2018**, *30*, 1804215. https://doi.org/10.1002/adma.201804215

[11] A. Way, J. Luke, A. D. Evans, Z. Li, J.-S. Kim, J. R. Durrant, H. K. H. Lee, W. C. Tsoi, *AIP Adv.* **2019**, *9*, 085220. https://doi.org/10.1063/1.5104333

[12] K. G. Godinho, B. J. Morgan, J. P. Allen, D. O. Scanlon, G. W. Watson, *J. Phys. Condens. Matter* **2011**, *23*, 334201. https://doi.org/10.1088/0953-8984/23/33/334201

[13] M.-G. Kim, M. G. Kanatzidis, A. Facchetti, T. J. Marks, *Nat. Mater.* **2011**, *10*, 382. https://doi.org/10.1038/nmat3011

[14] K. Rickert, A. Huq, S. H. Lapidus, A. Wustrow, D. E. Ellis, K. R. Poeppelmeier, *Chem. Mater.* **2015**, *27*, 8084. https://doi.org/10.1021/acs.chemmater.5b03790

[15] S. Flynn, A. J. Adekoya, S. Saeed, C. Zhang, V. P. Dravid, G. B. Gonzalez, K. R. Poeppelmeier, *Inorg. Chem* **2019**, *58*, 15610. https://doi.org/10.1021/acs.inorgchem.9b02692

[16] W. Huang, P. H. Chien, K. McMillen, S. Patel, J. Tedesco, L. Zeng, S. Mukherjee, B. Wang, Y. Chen, G. Wang, Y. Wang, Y. Gao, M. J. Bedzyk, D. M. DeLongchamp, Y. Y. Hu, J. E. Medvedeva, T. J. Marks, A. Facchetti, *Proc. Natl. Acad. Sci.* **2020**, *117*, 18231. https://doi.org/10.1073/pnas.2007897117

[17] Y. K. Naganovsky, S. E. Sigaryov, *Solid State Ionics* **1992**, *50*, 1. https://doi.org/10.1016/0167-2738(92)90030-S

[18] X. Zhao, Z. Zhang, X. Zhang, B. Tang, Z. Xie, Z. Zhou, *J. Mater. Chem. A* **2018**, *6*, 2625, https://doi.org/10.1039/C7TA08968F.

[19] S. Flynn, S. Sanghvi, M. L. Nisbet, K. J. Griffith, W. Zhang, P. S. Halasyamani, S. M. Haile, K. R. Poeppelmeier, *Chem. Mater.* **2020**, *32*, 4785. https://doi.org/10.1021/acs.chemmater.0c01491

[20] P. Shuk, H. D. Wiemhöfer, U. Guth, W. Göpel, M. Greenblatt, *Solid State Ionics* **1996**, *89*, 179. https://doi.org/10.1016/0167-2738(96)00348-7

[21] T. Takahashi, H. Iwahara, Y. Nagai, *J. Appl. Electrochem.* **1972**, *2*, 97. https://doi.org/10.1007/bf00609125

[22] X. Kuang, J. L. Payne, M. R. Johnson, I. Radosavljevic Evans, *Angew. Chem., Int. Ed.* **2012**, *51*, 690. https://doi.org/10.1002/anie.201106111

[23] M. T. Dunstan, D. M. Halat, M. L. Tate, I. R. Evans, C. P. Grey, *Chem. Mater.* **2019**, *31*, 1704. https://doi.org/10.1021/acs.chemmater.8b05143

[24] J. Goodenough, A. Manthiram, P. Paranthaman, Y. S. Zhen, *Solid State Ionics* **1992**, *52*, 105. https://doi.org/10.1016/0167-2738(92)90096-8

[25] N. Kim, C. P. Grey, *Science* **2002**, *297*, 1317. https://doi.org/10.1126/science.1074130

[26] M. Guignard, L. Albrecht, J. W. Zwanziger, *Chem. Mater.* **2007**, *19*, 286. https://doi.org/10.1021/cm062208a

[27] T. Maeder, *Int. Mater. Rev.* **2013**, *58*, 3. https://doi.org/10.1179/1743280412Y.0000000010

[28] M. Vehkamäki, T. Hatanpää, M. Kemell, M. Ritala, M. Leskelä, *Chem. Mater.* **2006**, *18*, 3883. https://doi.org/10.1021/cm060966v

[29] D. J. Singh, S. S. A. Seo, H. N. Lee, *Phys. Rev. B* **2010**, *82*, 180103. https://doi.org/10.1103/PhysRevB.82.180103

[30] H. G. Kim, T. T. Tran, W. Choi, T. S. You, P. S. Halasyamani, K. M. Ok, *Chem. Mater.* **2016**, *28*, 2424. https://doi.org/10.1021/acs.chemmater.6b00778

[31] F. Ding, M. L. Nisbet, H. Yu, W. Zhang, L. Chai, P. S. Halasyamani, K. R. Poeppelmeier, *Inorg. Chem.* **2018**, *57*, 7950. https://doi.org/10.1021/acs.inorgchem.8b01087

[32] K. M. Ok, *Chem. Commun.* **2019**, *55*, 12737. https://doi.org/10.1039/C9CC06778G

[33] R. W. Schurko, *Acc. Chem. Res.* **2013**, *46*, 1985. https://doi.org/10.1021/ar400045t

[34] D. C. Apperley, R. K. Harris, P. Hodgkinson, *Solid-State NMR: Basic Principles and Practice*, Monumentum Press, New York, NY **2012**.

[35] P. Pyykkö, *Mol. Phys.* **2018**, *116*, 1328. https://doi.org/10.1080/00268976.2018.1426131

[36] A. Y. H. Lo, T. E. Bitterwolf, C. L. B. Macdonald, R. W. Schurko, *J. Phys. Chem. A* **2005**, *109*, 7073. https://doi.org/10.1021/jp0521499

[37] O. B. Lapina, D. F. Khabibulin, A. A. Shubin, V. V. Terskikh, *Prog. Nucl. Magn. Reson. Spectrosc.* **2008**, *53*, 128. https://doi.org/10.1016/j.pnmrs.2007.12.001

[38] J. V. Hanna, K. J. Pike, T. Charpentier, T. F. Kemp, M. E. Smith, B. E. G. Lucier, R. W. Schurko, L. S. Cahill, *Chem. – Eur. J.* **2010**, *16*, 3222. https://doi.org/10.1002/chem.200901581

[39] K. E. Johnston, J. M. Griffin, R. I. Walton, D. M. Dawson, P. Lightfoot, S. E. Ashbrook, *Phys. Chem. Chem. Phys.* **2011**, *13*, 7565. https://doi.org/10.1039/C1CP20258H

[40] E. Papulovskiy, A. A. Shubin, V. V. Terskikh, C. J. Pickard, O. B. Lapina, *Phys. Chem. Chem. Phys.* **2013**, *15*, 5115. https://doi.org/10.1039/C3CP44016H

[41] K. J. Griffith, M. A. Hope, P. J. Reeves, M. Anayee, Y. Gogotsi, C. P. Grey, *J. Am. Chem. Soc.* **2020**, *142*, 18924. https://doi.org/10.1021/jacs.0c09044

[42] Y. Tomita, K. Yamada, H. Ohki, T. Okuda, *Z. für Naturforschung A* **1998**, *53*, 466. https://doi.org/10.1515/zna-1998-6-730

[43] Y. Tomita, K. Yamada, H. Ohki, T. Okuda, *Z. für Naturforschung A* **2002**, *57*, 447. https://doi.org/10.1515/zna-2002-6-728

[44] K. Yamada, K. Kumano, T. Okuda, *Solid State Ionics* **2005**, *176*, 823. https://doi.org/10.1016/j.ssi.2004.10.016

[45] K. Yamada, K. Kumano, T. Okuda, *Solid State Ionics* **2006**, *177*, 1691. https://doi.org/10.1016/j.ssi.2006.06.026

[46] G. Scholz, T. Krahl, M. Ahrens, C. Martineau, J. Y. Buzaré, C. Jäger, E. Kemnitz, *J. Fluorine Chem.* **2011**, *132*, 244. https://doi.org/10.1016/j.jfluchem.2011.01.010

[47] A. Karmakar, G. M. Bernard, A. Meldrum, A. O. Oliynyk, V. K. Michaelis, *J. Am. Chem. Soc.* **2020**, *142*, 10780. https://doi.org/10.1021/jacs.0c02198

[48] H. Hamaed, M. W. Laschuk, V. V. Terskikh, R. W. Schurko, *J. Am. Chem. Soc.* **2009**, *131*, 8271. https://doi.org/10.1021/ja901347k

[49] H. Hamaed, K. E. Johnston, B. F. T. Cooper, V. V. Terskikh, E. Ye, C. L. B. Macdonald, D. C. Arnold, R. W. Schurko, *Chem. Sci.* **2014**, *5*, 982. https://doi.org/10.1039/C3SC52809J

[50] F. Chen, G. Ma, G. M. Bernard, R. G. Cavell, R. McDonald, M. J. Ferguson, R. E. Wasylishen, *J. Am. Chem. Soc.* **2010**, *132*, 5479. https://doi.org/10.1021/ja100625p

[51] F. Chen, G. Ma, R. G. Cavell, V. V. Terskikh, R. E. Wasylishen, *Chem. Commun.* **2008**, *45*, 5933. https://doi.org/10.1039/b814326a

[52] A. Y. H. Lo, T. Jurca, D. S. Richeson, D. L. Bryce, *J. Phys. Chem. Lett.* **2010**, *1*, 3078. https://doi.org/10.1021/jz101241r
[53] R. E. Wasylishen, K. C. Wright, K. Eichele, T. S. Cameron, *Inorg. Chem.* **1994**, *33*, 407. https://doi.org/10.1021/ic00081a003
[54] K. Yamada, T. Yamaguchi, R. Ohashi, S. Ohki, K. Deguchi, K. Hashi, A. Goto, T. Shimizu, *Solid State Nucl. Magn. Reson.* **2020**, *109*, 101688. https://doi.org/10.1016/j.ssnmr.2020.101688
[55] T. J. Bastow, H. J. Whitfield, *J. Magn. Reson.* **1975**, *20*, 1. https://doi.org/10.1016/0022-2364(75)90144-4
[56] A. Faucher, V. V. Terskikh, R. E. Wasylishen, *Solid State Nucl. Magn. Reson.* **2014**, *61–62*, 54. https://doi.org/10.1016/j.ssnmr.2014.05.005
[57] K. J. D. Mackenzie, M. E. Smith, *Multinuclear Solid-State NMR of Inorganic Materials*, Pergamon Materials Series Vol. 6, Pergamon, London **2002**.
[58] Z. Gan, P. Srinivasan, J. R. Quine, S. Steuernagel, B. Knott, *Chem. Phys. Lett.* **2003**, *367*, 163. https://doi.org/10.1016/S0009-2614(02)01681-0
[59] C. M. Widdifield, D. L. Bryce, *J. Phys. Chem. A* **2010**, *114*, 10810. https://doi.org/10.1021/jp108237x
[60] C. M. Widdifield, A. D. Bain, D. L. Bryce, *Phys. Chem. Chem. Phys.* **2011**, *13*, 12413. https://doi.org/10.1039/c1cp20572b
[61] R. J. Attrell, C. M. Widdifield, I. Korobkov, D. L. Bryce, *Cryst. Growth Des.* **2012**, *12*, 1641. https://doi.org/10.1021/cg201683p
[62] F. A. Perras, D. L. Bryce, *Angew. Chem., Int. Ed.* **2012**, *51*, 4227. https://doi.org/10.1002/anie.201200728
[63] F. A. Perras, C. M. Widdifield, D. L. Bryce, *Solid State Nucl. Magn. Reson.* **2012**, *45–46*, 36. https://doi.org/10.1016/j.ssnmr.2012.05.002
[64] C. M. Widdifield, F. A. Perras, D. L. Bryce, *Phys. Chem. Chem. Phys.* **2015**, *17*, 10118. https://doi.org/10.1039/C5CP00602C
[65] O. Pecher, D. M. Halat, J. Lee, Z. Liu, K. J. Griffith, M. Braun, C. P. Grey, *J. Magn. Reson.* **2017**, *275*, 127. https://doi.org/10.1016/j.jmr.2016.12.008
[66] D. L. Bryce; R. E. Wasylishen Quadrupolar nuclei in solids: influence of different interactions on spectra. In *Encyclopedia of Magnetic Resonance*; Harris, R. K., Ed.; John Wiley & Sons, Ltd: Chichester, UK, **2011**. https://doi.org/10.1002/9780470034590.emrstm1197
[67] A. D. Bain, M. Khasawneh, *Concepts Magn. Reson.* **2004**, *22A*, 69. https://doi.org/10.1002/cmr.a.20013
[68] A. D. Bain, *Magn. Reson. Chem.* **2017**, *55*, 198. https://doi.org/10.1002/mrc.4418
[69] D. Massiot, I. Farnan, N. Gautier, D. Trumeau, A. Trokiner, J. P. Coutures, *Solid State Nucl. Magn. Reson.* **1995**, *4*, 241. https://doi.org/10.1016/0926-2040(95)00002-8
[70] P. K. Allan, J. M. Griffin, A. Darwiche, O. J. Borkiewicz, K. M. Wiaderek, K. W. Chapman, A. J. Morris, P. J. Chupas, L. Monconduit, C. P. Grey, *J. Am. Chem. Soc.* **2016**, *138*, 2352. https://doi.org/10.1021/jacs.5b13273
[71] H. J. Jakobsen, J. Skibsted, H. Bildsøe, N. C. Nielsen, *J. Magn. Reson.* **1989**, *85*, 173. https://doi.org/10.1016/0022-2364(89)90333-8
[72] R. K. Harris, E. D. Becker, *Pure Appl. Chem.* **2008**, *80*, 59. https://doi.org/10.1351/pac200880010059
[73] S. Sturniolo, T. F. G. Green, R. M. Hanson, M. Zilka, K. Refson, P. Hodgkinson, S. P. Brown, J. R. Yates, *Solid State Nucl. Magn. Reson.* **2016**, *78*, 64. https://doi.org/10.1016/j.ssnmr.2016.05.004
[74] S. J. Clark, M. D. Segall, C. J. Pickard, P. J. Hasnip, M. I. J. Probert, K. Refson, M. C. Payne, *Z. für Krist.* **2005**, *220*, 567. https://doi.org/10.1524/zkri.220.5.567.65075
[75] C. J. Pickard, F. Mauri, *Phys. Rev. B* **2001**, *63*, 245101. https://doi.org/10.1103/PhysRevB.63.245101
[76] J. R. Yates, C. J. Pickard, F. Mauri, *Phys. Rev. B* **2007**, *76*, 024401. https://doi.org/10.1103/PhysRevB.76.024401
[77] M. Profeta, F. Mauri, C. J. Pickard, *J. Am. Chem. Soc.* **2003**, *125*, 541. https://doi.org/10.1021/ja027124r
[78] J. P. Perdew, K. Burke, M. Ernzerhof, *Phys. Rev. Lett.* **1996**, *77*, 3865. https://doi.org/10.1103/PhysRevLett.77.3865
[79] D. Vanderbilt, *Phys. Rev. B* **1990**, *41*, 7892. https://doi.org/10.1103/PhysRevB.41.7892
[80] D. D. Koelling, B. N. Harmon, *J. Phys. C Solid State Phys.* **1977**, *10*, 3107. https://doi.org/10.1088/0022-3719/10/16/019
[81] H. J. Monkhorst, J. D. Pack, *Phys. Rev. B* **1976**, *13*, 5188. https://doi.org/10.1103/PhysRevB.13.5188
[82] V. K. Michaelis, S. Kroeker, *J. Phys. Chem. C* **2010**, *114*, 21736. https://doi.org/10.1021/jp1071082
[83] S. Sene, B. Bouchevreau, C. Martineau, C. Gervais, C. Bonhomme, P. Gaveau, F. Mauri, S. Bégu, P. H. Mutin, M. E. Smith, D. Laurencin, *CrystEngComm* **2013**, *15*, 8763. https://doi.org/10.1039/c3ce40981c
[84] V. R. Seymour, J. M. Griffin, B. E. Griffith, S. J. Page, D. Iuga, J. V. Hanna, M. E. Smith, *J. Phys. Chem. C* **2020**, *124*, 23976. https://doi.org/10.1021/acs.jpcc.0c07281
[85] D. S. Middlemiss, R. Blanc, C. J. Pickard, C. P. Grey, *J. Magn. Reson.* **2010**, *204*, 1. https://doi.org/10.1016/j.jmr.2010.01.004
[86] S. L. Tagg, R. E. Youngman, J. W. Zwanziger, *J. Phys. Chem.* **1995**, *99*, 5111. https://doi.org/10.1021/j100014a035
[87] E. A. Kravchenko, V. G. Orlov, M. P. Shlykov, *Russ. Chem. Rev.* **2006**, *75*, 77. https://doi.org/10.1070/RC2006v075n01ABEH003596
[88] L. A. O'Dell, R. W. Schurko, *Chem. Phys. Lett.* **2008**, *464*, 97. https://doi.org/10.1016/j.cplett.2008.08.095
[89] L. A. O'Dell, A. J. Rossini, R. W. Schurko, *Chem. Phys. Lett.* **2009**, *468*, 330. https://doi.org/10.1016/j.cplett.2008.12.044
[90] L. A. O'Dell, *Solid State Nucl. Magn. Reson.* **2013**, *55–56*, 28. https://doi.org/10.1016/j.ssnmr.2013.10.003

SUPPORTING INFORMATION

Additional supporting information may be found online in the Supporting Information section at the end of this article.

How to cite this article: K. J. Griffith, F. Ding, S. Flynn, *Magn Reson Chem* **2021**, 1. https://doi.org/10.1002/mrc.5183